

# Effect of resist on the transfer of line-edge roughness spatial metrics from mask to wafer

Patrick P. Naulleau<sup>1</sup> and Gregg M. Gallatin<sup>2</sup>

<sup>1</sup>Center for X-Ray Optics, Lawrence Berkeley National Laboratory, Berkeley, CA 94720

<sup>2</sup>Center for Nanoscale Science and Technology, NIST, Gaithersburg, MD 20899

## Abstract

Mask contributors to line-edge roughness (LER) have recently been shown to be an issue of concern for extreme ultraviolet lithography both in terms of the accuracy of current resist evaluation tests as well the ultimate LER requirements for the 22-nm production node and beyond. More recently, it has been shown that the power spectral density of the mask-induced roughness, is markedly different than that of intrinsic resist roughness and thus potentially serves as a mechanism for distinguishing mask effects from resist effects in experimental results. But the evaluation of stochastic effects in the resist itself demonstrate that such a test would only be viable in cases where the resist effects are completely negligible in terms of their contribution to the total LER compared to the mask effects. On the other hand the results presented here lead us to the surprising conclusion that it is indeed possible for mask contributors to be the dominant source of LER while the spatial characteristics of the LER remain indistinguishable from the fractal characteristics of resist-induced LER.

**Keyword:** extreme ultraviolet, lithography, multilayer, mask, line-edge roughness

## **Introduction**

Mask errors such as pattern line-edge roughness (LER) [1] and reflective multilayer roughness [2, 3] have recently been shown [4] to potentially limit the ability to accurately determine resist-contributors to wafer-based LER measurements. This is particularly true for extreme ultraviolet (EUV) lithography where mask surface roughness can lead to significant levels of image plane speckle and hence LER. It has also been shown [5] that the mask errors affect the shape of the power spectral density (PSD) and therefore LER spatial metrics such as the correlation length and roughness exponent [6-8]. It has been suggested [5] that the significant change in morphology of the PSD between mask and resist effects could provide a mechanism to distinguish between mask-induced LER and intrinsic resist LER. The feasibility and resolution of the PSD-based root-cause analysis approach, however, further depends on how the resist itself transfers the aerial image roughness studied in Ref. [5].

Here we explicitly evaluate the contribution of mask LER to the net resist LER using the magnitude and spatial scaling characteristics of the PSD and the height-height correlation function. This contribution is considered both with and without stochastic effects in the resist, i.e. both with and without the intrinsic cause of resist LER. By varying the relative amounts of the two contributions we study how this changes the measured metrics and consider the feasibility of distinguishing mask and resist effects in practice.

## **Modeling overview**

The aerial-image modeling method used in this study has previously been described in the literature [4, 5] and is only briefly summarized here. Thin mask modeling is used with the multilayer surface roughness being represented as a random phase error in the clear area of the pattern. Because the study of LER requires the modeling of a large two dimensional area with high resolution both in the mask plane and the wafer plane, full three-dimensional modeling is

not feasible. For example, to compute the  $2\ \mu\text{m} \times 2\ \mu\text{m}$  image-plane lateral area required for accurate LER characterization and the depth structure of the EUV mask as would be required to model the multilayer roughness, the memory requirement for the  $5\times$  mask of interest here would be well over a terabyte. In the thin mask model, the absorber is modeled as infinitesimally thin and the multilayer is modeled as a random phase plane to represent the replicated multilayer roughness. This approach for multilayer roughness or defect modeling is known as the single-surface approximation [9] and has been shown to be quite effective. In the thin mask model, the entire mask is decomposed to a single complex-valued plane.

Figure 1 shows a three-dimensional representation of an example mask including the two roughness components of concern. Both the absorber LER and multilayer surface roughness are greatly exaggerated for illustrative purposes. The absorber LER can be thought of a lateral roughness whereas the multilayer roughness is longitudinal. The multilayer reflectivity is assumed to be uniform over the surface with the only effect of the roughness being a phase shift imparted upon reflection. The single-surface approximation treats the light field as being reflected directly from the top surface of the multilayer thus the phase shift in waves is simply determined geometrically as  $2\times$  the surface height deviation divided by the wavelength (13.5 nm). Evidently, quite small surface perturbations can lead to significant phase shifts: a height of only 1.7 nm leads to a  $\lambda/4$  phase shift.

For the generation of the actual mask data used in the simulations to follow, the morphology of the absorber LER is set to match that measured using scanning electron micrographs (SEMs) on a real mask and the phase roughness morphology is determined from atomic force microscopy [4]. The flare and wavefront aberrations used in the modeling are based on published results from the SEMATECH Berkeley microfield exposure tool (MET) [10-13]. It

should be noted that projection optics flare has previously been shown not to be a significant contributor to image-plane LER [4].

### Resist LER transfer without stochastic effects

We begin by exploring the effect of the resist mean-field transfer function on the image plane LER, initially ignoring stochastic effects arising from the resist itself and/or photon arrival statistics. Resist exposure, bake and development at a fundamental level is a highly nonlinear process which is described by a complex set of coupled nonlinear reaction-diffusion equations. Nevertheless, in spite of this complexity, it often turns out that a useful and reasonably accurate method of representing resist behavior is to treat it as a linear system with the resist response being represented by a point-spread function (PSF) [14-25]. Unfortunately this approximation is not sufficient to accurately evaluate variations on the order of a nm which we need to do here and so the full nonlinearity of both the exposure process and the post exposure bake process are incorporated into the model.

Acid release during exposure can be described by the equation

$$\begin{aligned} \frac{\partial \rho_{Acid}(\vec{r}, t)}{\partial t} &= -\alpha I(\vec{r}, t) q \rho_{PAG}(\vec{r}, t) \\ &= -\alpha I(\vec{r}, t) q (\rho_{PAG0} - \rho_{Acid}(\vec{r}, t)) \end{aligned} \quad (1)$$

Here  $\alpha$  is the absorptivity of the resist in units of 1/length,  $I(\vec{r}, t)$  is the intensity in units of the number of photons per unit area per unit time at position  $\vec{r} = (x, y, z)$  at exposure time  $t$ ,  $\rho_{PAG}(\vec{r}, t)$  is the number of photoacid generator (PAG) molecules per unit volume,  $\rho_{Acid}(\vec{r}, t)$  is the number of acid molecules per unit volume, and  $q$  is a scale factor with units of volume. This equation can be understood as follows. The number photons absorbed per unit time in a small

volume of cross-sectional area  $A$  and length  $L$  is given by  $\alpha IAL$ . In an EUV resist the absorbed photons generate photoelectrons. If these photoelectrons interact with a PAG molecule they cause it to release an acid. It is reasonable to assume that the probability of a photoelectron interacting with a PAG molecule increases with the density of PAG molecules. We will take this dependence to be linear and so the number of acids created in volume  $AL$  per each absorbed photon is given by  $q\rho_{PAG}$  with  $q$  a volumetric scale factor. Thus, the quantum efficiency of the process,  $Q$ , defined as the number of acids released per absorbed photon is  $Q = q\rho_{PAG}$ . Multiplying the number of acids generated per absorbed photon times the number of absorbed photons and dividing through by the volume  $AL$  we get that the number of acids generated per unit volume per unit time is  $\alpha Iq\rho_{PAG}$ . Assuming each PAG molecule can release one and only one acid the total of the number of PAG and acid molecules must be a constant, i.e.,

$$\rho_{PAG0} = \rho_{Acid}(\vec{r}, t) + \rho_{PAG}(\vec{r}, t) \quad (2)$$

where  $\rho_{PAG0} = \rho_{PAG}(\vec{r}, t = 0)$  is the nominally spatially uniform initial PAG loading in the resist.

Using this conservation law yields the second line in Eq (1) and solving Eq (1) yields

$$\rho_{Acid}(\vec{r}, t) = \rho_{PAG0} \left[ 1 - \exp\left[-\alpha q E(\vec{r}, t)\right] \right] \quad (3)$$

where  $E(\vec{r}, t) = \int_0^t dt I(\vec{r}, t)$  is the exposure dose at position  $\vec{r}$  at time  $t$ .

The effect of the post exposure bake (PEB) is to smear or blur  $\rho_{Acid}(\vec{r}, t)$  since during PEB each acid performs a diffusive random walk through the resist. As each acid diffuses it catalyzes deprotection of the resist polymer, i.e., converts it from insoluble to soluble for a positive tone resist and vice versa for a negative tone resist. Let  $t$  now refer to the PEB time instead of the exposure time. Then at the beginning of the PEB the acid density distribution is

given by

$$\rho_{Acid0}(\vec{r}) = \rho_{PAG0} [1 - \exp[-\alpha q E(\vec{r})]] \quad (4)$$

where  $E(\vec{r})$  is the total exposure dose.

We first discuss the process of acid diffusion in the absence of base quencher. The effect base quencher is discussed below.

When no base is present the process of acid diffusion and deprotection can be modeled by the pair of equations

$$\begin{aligned} \frac{\partial \rho_P(\vec{r}, t)}{\partial t} &= -k \rho_{Acid}(\vec{r}, t) \rho_P(\vec{r}, t) \\ \frac{\partial \rho_{Acid}(\vec{r}, t)}{\partial t} &= D \nabla^2 \rho_{Acid}(\vec{r}, t) \end{aligned} \quad (5)$$

where a constant diffusivity has been assumed. Here  $\rho_P(\vec{r}, t)$  denotes the density of protected (insoluble) resist polymer,  $k$  is a reaction rate constant with units of length<sup>d</sup>/time when working in  $d$  space dimensions,  $D$  is the standard diffusion constant and  $t$  now represents the PEB time and not the exposure time. Assuming no resist shrinkage or outgassing the sum of the protected  $\rho_P$  and deprotected  $\rho_D$  polymer densities must equal the initially uniform resist density  $\rho_0$ , i.e.,  $\rho_P(\vec{r}, t) + \rho_D(\vec{r}, t) = \rho_0$ . Solving Eq(5) for  $\rho_P(\vec{r}, t)$  and using  $\rho_P = \rho_0 - \rho_D$  gives

$$\bar{\rho}_D(\vec{r}, t) \equiv \frac{\rho_D(\vec{r}, t)}{\rho_0} = 1 - \exp\left[-k \int d^3 r' PSF(\vec{r} - \vec{r}', t) \rho_{Acid0}(\vec{r}')\right] \quad (6)$$

where  $\bar{\rho}_D(\vec{r}, t)$  is the fraction of deprotected resist,  $PSF(\vec{r} - \vec{r}', t)$  is the reaction diffusion point spread function defined in 3D by

$$PSF(\vec{r}, t) = \int_0^{\infty} dt \frac{1}{4\pi Dt} \exp\left[-\vec{r}^2 / 4Dt\right] \quad (7)$$

The final step of resist development will be represented using a simple deprotection threshold model, i.e., resist at positions  $\vec{r}$  with  $\rho_D(\vec{r})$  greater than the threshold value will be assumed to wash away during development while resist at positions  $\vec{r}$  with  $\rho_D(\vec{r})$  less than the threshold value will be assumed to remain. The threshold value is chosen to give the measured feature size at the given dose. More detailed models for development do exist [25] and could be used but the deprotection threshold model will suffice here. Note that expanding all exponents in the above expressions to first order yields

$$\bar{\rho}_D(\vec{r}, t) \approx k\alpha q \rho_{PAG0} \int d^3r' PSF(\vec{r} - \vec{r}', t) E(\vec{r}') \quad (8)$$

which is the standard result when using the linear PSF approach.

The  $dt$  integral in Eq (7) is easily evaluated for three dimensions,  $d = 3$ , and substituting into Eq (6) gives

$$\bar{\rho}_D(\vec{r}, t) = 1 - \exp\left[-\frac{k}{4\pi D} \int d^3r' \left(1 - \operatorname{erf}\left(\frac{|\vec{r} - \vec{r}'|}{2\sqrt{Dt}}\right)\right) \frac{\rho_{Acid0}(\vec{r}')}{|\vec{r} - \vec{r}'|}\right] \quad (9)$$

where  $\operatorname{erf}(\dots)$  is the error function and  $R \equiv \sqrt{Dt}$  is the diffusion range or resist blur.

Since 3D is numerically expensive we will reduce the problem to 2D. This allows us to use standard two dimensional aerial images. To achieve this reduction assume that the dose  $E(\vec{r})$  is independent of  $z$ , i.e.,  $E(\vec{r}) \equiv E(x, y, z) \rightarrow E(x, y)$  which implies that  $\bar{\rho}_{Acid}(\vec{r}, t) \rightarrow \bar{\rho}_{Acid}(x, y, t)$  and so

$$\bar{\rho}_D(\mathbf{r}, t) \rightarrow \bar{\rho}_D(\mathbf{r}, y, t) = 1 - \exp\left[-k \int dx' dy' PSF_{2D}(\mathbf{r} - x', y - y', t) \bar{\rho}_{Acid0}(\mathbf{r}', y')\right] \quad (10)$$

where

$$PSF_{2D}(\mathbf{r}, y, t) = \int_{-H/2}^{+H/2} PSF(\mathbf{r}, t) dz \quad (11)$$

with  $H$  the resist thickness. For the case where  $H \gg R$  we can take the  $z$  integral to range from  $-\infty$  to  $+\infty$ .

It should be noted that in the linearized case if we integrate 2 dimensions of the 3D PSF given above to reduce it to the 1D PSF, the result matches the experimentally measured shape [15] of the 1D PSF which also matches the shape of the 1D deprotection density derived from a full numerical simulation of the reaction diffusion equations [18]. We note that the same 1D PSF equation as given in Ref [17] was derived independently in Ref [26].

Finally the above analysis accounts only for the mean or average behavior of what is a stochastic system. Stochastic effects occur during the exposure, PEB and development steps. Here we include only stochastic exposure effects. The justification for making this approximation comes from fact that LER is dominated by low spatial frequencies and the stochastic effects from exposure alone account for this [17].

To handle the effect of base quencher Eq (5) must be replaced by [25]

$$\begin{aligned} \frac{\partial \bar{\rho}_P(\mathbf{r}, t)}{\partial t} &= -k \rho_{Acid}(\mathbf{r}, t) \bar{\rho}_P(\mathbf{r}, t) \\ \frac{\partial \rho_{Acid}(\mathbf{r}, t)}{\partial t} &= D_{Acid} \nabla^2 \rho_{Acid}(\mathbf{r}, t) - g \rho_{Acid}(\mathbf{r}, t) \bar{\rho}_{Base}(\mathbf{r}, t) \\ \frac{\partial \rho_{Base}(\mathbf{r}, t)}{\partial t} &= D_{Base} \nabla^2 \rho_{Base}(\mathbf{r}, t) - g \rho_{Acid}(\mathbf{r}, t) \bar{\rho}_{Base}(\mathbf{r}, t) \end{aligned} \quad (12)$$

where  $\rho_{Base}(\mathbf{r}, t)$  is the density of base in units of the number of base molecules per unit volume.

The cross-term  $g\rho_{Acid}\rho_{Base}$  accounts for the acid and base molecules neutralizing each other with the coupling constant  $g$  (units in 3D = volume/time) governing the rate of the reaction. Note that we have divided the first equation by  $\rho_0$  and so are working with the local fraction of protected polymer,  $\bar{\rho}_p$ .

The cross-term makes the equations inherently nonlinear and so not analytically solvable in a general form. We will numerically solve them using the approach of Fukuda [27] in which the solution is generated by alternating between the diffusion and reaction processes, i.e., diffuse with no reaction for a time  $\Delta t$  followed by reaction without diffusion for the same time. Continue alternating between these two processes until the sum of the time steps  $\Delta t$  equals the total PEB time. The results presented below were generated using four steps, two reaction and two diffusion with the assumptions that the base does not diffuse and that the reaction proceeds fast enough that acid and base neutralize each other during the reaction step. A derivation of acid base neutralization in the fast reaction case is given in the Appendix.

Figure 2 shows the computed aerial image intensity given a mask matching the absorber and surface statistics of a typical EUV mask [4]. The illumination condition is annular for an inner  $\sigma$  of 0.35 and an outer  $\sigma$  of 0.55 and the image is computed at best focus. This aerial image can then be convolved with the PSF from Eq. [3] to determine the deprotection image from which we can measure the LER and hence the effect of the resist PSF. This process is repeated ten times with ten independent realizations of the rough mask and the resulting LER power spectral density (PSD) is averaged. Figures 3 and 4 show the resulting PSDs and height-height correlation functions (HHCF) [7] as a function of  $R$  and  $k$ , respectively. In Fig. 3,  $k$  is assumed to be  $4 \text{ nm}^3/\text{s}$  and in Fig. 4,  $R$  is assumed to be 15 nm. In both cases,  $t$  is set to 60 seconds. For comparison, the plots also show the PSD of typical resist roughness which is self-affine in

nature.

The results in Figs. 3 and 4 show that  $R$  and  $k$  have minimal effect the morphology of the LER power spectrum and even less on the HHCF. Nevertheless, the lateral shifts in the HHCF plots indicate an apparent shift in correlation length is observed both as a function of  $R$  and  $k$ . Previous analysis [5] demonstrated that one potential mechanism for distinguishing mask roughness from resist roughness was to compare the roughness exponent ( $\alpha$ ) as measured from the PSD and the HHCF [7]. The method relies on the fact that resist-induced LER is expected to be self-affine in nature in which case the relationship between the rising slope of the HHCF and the falling slope of the PSD is well defined. For self-affine roughness (which, by definition, follows a power-law behavior) the roughness exponent is determined from the log-log slope of the HHCF and is related to the log-log slope of the PSD through the relationship  $\alpha = (\text{Slope}_{\text{PSD}} - 1)/2$ . Modeling has shown [5] that the mask-induced LER is not self-affine as is evident by observation of the PSD. Modeling has also shown, however, that it is difficult to distinguish mask-induced LER from self-affine roughness using the HHCF which exhibits no significant change in morphology when used to analyze mask-induced roughness instead of self-affine (resist) roughness. The slope of the PSD is much more strongly affected by the mask-induced roughness than is the slope of the HHCF, thus comparing the relationships between these two slopes (or the extracted  $\alpha$  values) allows for the presence of mask-induced roughness to be observed.

Table 1 shows a comparison of the roughness exponent measured from the PSD and HHCF for the various resist blur parameters used in Figs. 3 and 4. The first row in the table corresponds to the mask roughness itself (no resist blur applied). For the PSD, the roughness exponent is measured from the region of spatial frequencies much greater than the reciprocal of

the correlation length as determined from the autocorrelation function or the HHCF. In general this corresponds to spatial frequencies ranging approximately from  $50 \mu\text{m}^{-1}$  to  $200 \mu\text{m}^{-1}$ . Referring to Fig. 3, it is evident that this is beyond the frequency range wherein the morphology changes most significantly as a function of resist blur, thus we see minimal change in the PSD-measured roughness exponent. This shows that the PSD roughness exponent alone cannot be used as an indicator of the dominance of mask-induced LER. We note, however, that a PSD slope metric with higher sensitivity to the resist blur could readily be achieved if instead of considering the roughness exponent, we characterized the high-slope region of the PSD which falls at frequencies considerably lower than those used to characterize the roughness exponent.

For the HHCF, the roughness exponent is measured from the region of spatial separations less than the correlation length. In general this corresponds to offsets of approximately 5 nm to 30 nm. Although the results show some variation of the HHCF roughness exponent with resist blur, the effect is quite small and does not appear to be systematic. It is interesting to note that the sensitivity of the mask-induced LER PSD to the resist blur parameters suggests the potential for an alternative method for determining these parameters based on the printing of a programmed roughness mask.

Since the resist blur has a significant impact on the PSD, one might also expect the blur to reduce the mask-induced LER magnitude. Table 1 also shows the LER values for the various blur settings. Although some effect on LER magnitude is observed, it is certainly small compared to the measurement uncertainty. This is a consequence of the majority of the mask-induced LER coming from low frequencies that are not affected by the resist blur. We also see that in some cases the LER is actually increased which would be impossible in a strictly linear system. As described above despite the deprotection blur itself being treated as a linear point

spread function, the saturation effects also captured in the modeling methodology described enable this characteristic. The increase in LER is seen in the case where the blur is very large presumably causing the harmful effects of reduced deprotection slope to outweigh any improvements caused by filtering the LER.

### **Resist LER transfer with stochastics**

Finally we consider the effects of the resist stochastics on the total LER PSD. The resist stochastics are modeled using the methodology presented in Ref. [17] and expanded on above. Essentially the model chooses the actual number of photons absorbed in each pixel randomly from a Poisson distribution whose mean corresponds to the aerial image intensity in that pixel. We assume a diffusion range of 10 nm and deprotection rate of 4 nm<sup>3</sup>/s. We look at the resulting PSD as a function of resist sensitivity since the stochastics vary with sensitivity. The sensitivity of the resist is changed in the model by changing base loading while keeping all other parameters constant. We note that the base-loading method for varying sensitivity is often used in experimental studies as well [28-30]. Figure 5 shows the resulting PSDs and HHCFs for dose to size values on 50 nm lines and spaces of 2 mJ/cm<sup>2</sup> through 128 mJ/cm<sup>2</sup>. The plots result from averaging over ten independent simulations with each simulation representing a separate independent realization of both the mask and resist stochastics. For high sensitivity cases, the characteristic morphology of mask-induced PSD is lost in the fractal resist PSD. At a dose to size values of approximately 32 mJ/cm<sup>2</sup> we begin to observe a slight deviation from fractal behavior indicative of mask-induced LER. No similar change in morphology is observed in the HHCFs plots. We can gain even further insight into the effect of the resist stochastics on the mask-induced LER by characterizing the roughness exponent and LER as a function of sensitivity (Table 2). The results show that it is difficult to identify the presence of the mask-induced LER

from the roughness exponent which, from the PSD, is measured based on the slope at spatial periods much shorter than the correlation length. Thus, to see the impact of the mask we must observe the PSD morphology or potentially use a different PSD metric which, for example, as mentioned above could be based on the slope of the PSD in the high slope region near the knee.

Figure 5 and Table 2 show that the mask effects only become evident when the mask-induced LER is so dominant that it accounts for nearly 100% of the total LER. Taking the 32 mJ/cm<sup>2</sup> value as representing the absolute minimum sensitivity required to observe any signature of mask effects in the PSD, we find the corresponding total LER to be 2.6 nm. Noting that the contributions from the mask alone correspond to 2.2 nm, the maximum tolerable resist LER (assuming quadrature addition) is approximately 1.4 nm or roughly one half of the mask LER. This condition would be necessary in order to observe the presence of mask-induced LER in the total PSD. In summary, an extremely low LER resist process would be required to enable the use of LER spatial scaling characteristics to be used as a metric for mask-induced LER in the resist image.

## **Discussion**

Previous aerial-image modeling results have shown the importance of mask-induced LER and suggested methods for experimentally determining the presence of these effects. Adding stochastic resist effects to the model, however, shows the previously proposed methods to be viable only in cases where the resist effects are negligible in terms of their contribution to the total LER compared to the mask contribution. Moreover, the results presented here lead us to the surprising conclusion that it is indeed possible for mask contributors to be the dominant source of wafer plane LER while the spatial characteristics of the wafer plane LER remain indistinguishable from the fractal characteristics of resist-induced LER.

This work was funded in part by SEMATECH, the authors are grateful to Warren Montgomery for program support. This work was partially carried out at Lawrence Berkeley National Laboratory, which is supported by the Director, Office of Science, Office of Basic Energy Sciences, of the U.S. Department of Energy under Contract No. DE-AC02-05CH11231.

## Appendix

Assume that  $g$  is large enough so that acid base neutralization takes place much faster than diffusion. In this limit the pair of acid and base equations reduce to

$$\begin{aligned}\frac{\partial \rho_{Acid}(\mathbf{r}, t)}{\partial t} &\cong -g \rho_{Acid}(\mathbf{r}, t) \rho_{Base}(\mathbf{r}, t) \\ \frac{\partial \rho_{Base}(\mathbf{r}, t)}{\partial t} &\cong -g \rho_{Acid}(\mathbf{r}, t) \rho_{Base}(\mathbf{r}, t)\end{aligned}\quad (13)$$

This pair of equations can be solved analytically but we do not need the full solution since we have assumed that the neutralization reaction happens very quickly and so we only need the final values of the densities. We can get these by subtracting one equation from the other which shows that  $\rho_{Acid}(\mathbf{r}, t) - \rho_{Base}(\mathbf{r}, t)$  is independent of time and so the difference at time  $t$  is equal to the difference at  $t = 0$ ,

$$\rho_{Acid}(\mathbf{r}, t) - \rho_{Base}(\mathbf{r}, t) \cong \rho_{Acid}(\mathbf{r}, 0) - \rho_{Base}(\mathbf{r}, 0) \quad (14)$$

The position dependence of  $\rho_{Acid}(\mathbf{r}, 0)$  is the latent image in the resist and as usual we will assume the base is uniformly distributed initially so that  $\rho_{Base}(\mathbf{r}, 0)$  doesn't depend on position,  $\rho_{Base}(\mathbf{r}, 0) \cong \rho_{Base0}$ . Solving Eq (14) for  $\rho_{Base}(\mathbf{r}, t)$  and substituting into Eq (13) gives

$$\frac{\partial \rho_{Acid}(\mathbf{r}, t)}{\partial t} \cong -g \rho_{Acid}(\mathbf{r}, t) (\rho_{Acid}(\mathbf{r}, t) - \rho_{Acid}(\mathbf{r}, 0) + \rho_{Base0}) \quad (15)$$

Given the rapid neutralization rate, i.e., large  $g$ , the neutralization will be complete in a short

time  $\tau$ , i.e.,  $\frac{\partial \rho_{Acid}(x, t = \tau)}{\partial t} \rightarrow 0$  with  $\tau$  small compared to the total PEB time,  $t_{PEB}$ . But since densities are never negative there are two distinct ways the right hand side of Eq (15) can be zero. For positions where  $\rho_{Base0} > \rho_{Acid}(x, 0)$  we have  $\rho_{Acid}(x, \tau) = 0$  while for positions where  $\rho_{Acid}(x, 0) > \rho_{Base0}$  we have  $\rho_{Acid}(x, \tau) = \rho_{Acid}(x, 0) - \rho_{Base0}$ . For  $\tau \ll t_{PEB}$  we can replace  $\rho_{Acid}(x, 0)$  as the acid distribution at the start of PEB with  $\rho_{Acid}(x, \tau) - \rho_{Base0} \approx \rho_{Acid}(x, 0) - \rho_{Base0}$  wherever this is positive and with 0 otherwise and proceed with the PEB as in the no base case.

## References

1. P. Naulleau and G. Gallatin, "The line-edge roughness transfer function and its application to determining mask effects in EUV resist characterization," *Appl. Opt.* **42**, 3390-3397 (2003).
2. N. Beaudry, T. Milster, "Effects of mask roughness and condenser scattering in EUVL systems," *Proc. SPIE.* **3676**, 653-662 (1999).
3. P. Naulleau, "The relevance of mask-roughness-induced printed line-edge roughness in recent and future EUV lithography tests," *Appl. Opt.* **43**, 4025-4032 (2004).
4. P. Naulleau, D. Niakoula, G. Zhang, "System-level line-edge roughness limits in extreme ultraviolet lithography," *J. Vac. Sci. & Technol. B* **26**, 1289-1293 (2008).
5. P. Naulleau and G. Gallatin, "Spatial scaling metrics of mask-induced line-edge roughness," *J. Vac. Sci. & Technol. B* **26**, 1903-1910 (2008).
6. D. He, F. Cerrina, "Process dependence of roughness in a positive-tone chemically amplified resist," *J. Vac. Sci. & Technol. B* **16**, 3748-3751 (1998).

7. V. Constantoudis, G. P. Patsis, A. Tserepi, E. Gogolides, "Quantification of line-edge roughness of photoresists. II. Scaling and fractal analysis and the best roughness descriptors," *J. Vac. Sci. & Technol. B* **21**, 1019-1026 (2003).
8. B. Bunday, M. Bishop, D. McCormack, "Determination of optimal parameters for CD-SEM measurement of line-edge roughness," *Proc. SPIE* **5375**, 515-533 (2004).
9. E. Gullikson, C. Cerjan, D. Stearns, P. Mirkarimi, D. Sweeney, "Practical approach for modeling extreme ultraviolet lithography mask defects," *J. Vac. Sci. Technol. B* **20**, 81-86 (2002).
10. J. Cain, P. Naulleau, E. Gullikson, C. Spanos, "Lithographic characterization of the flare in the Berkeley 0.3-numerical aperture extreme ultraviolet microfield optic," *J. Vac. Sci. & Technol. B* **24**, 1234-1237 (2006).
11. K. Goldberg, P. Naulleau, P. Denham, S. Rekawa, K. Jackson, E. Anderson and J. Liddle, "At-Wavelength Alignment and Testing of the 0.3 NA MET Optic," *J. Vac. Sci. & Technol. B* **22**, 2956-2961 (2004).
12. P. Naulleau, J. Cain, K. Goldberg, "Lithographic characterization of the spherical error in an EUV optic using a programmable pupil fill illuminator," *Appl. Opt.* **45**, 1957-1963 (2006).
13. P. Naulleau, J. Cain, K. Goldberg, "Lithographic characterization of the field dependent astigmatism and alignment stability of a 0.3 numerical aperture EUV microfield optic," *J. Vac. Sci. & Technol. B* **23**, 2003-2006 (2005).
14. C. Ahn, H. Kim, K. Baik, "A novel approximate model for resist process," *Proc. SPIE* **3334**, 752-763 (1998).
15. J. Hoffnagle, W. Hinsberg, M. Sanchez, and F. Houle, "Method of measuring the spatial resolution of a photoresist," *Opt. Lett.* **27**, 1776-1778, (2002).

16. P. Naulleau, "Verification of point-spread-function-based modeling of an extreme ultraviolet photoresist," *Appl. Opt.* **43**, 788–792, (2004).
17. G. Gallatin, "Resist blur and line edge roughness," *Proc. SPIE* **5754**, 38-52 (2005).
18. F. Houle, W. Hinsberg, M. Morrison, M. Sanchez, G. Wallraff, C. Larson, and J. Hoffnagle, "Determination of coupled acid catalysis-diffusion processes in a positive-tone chemically amplified photoresist," *J. Vac. Sci. Technol. B* **18**, 1874-1885 (2000).
19. see for example: Rodney Loudon, "The quantum theory of light", Clarendon Press, Oxford, 1983.
20. W. Hinsberg, F. Houle, M. Sanchez, J. Hoffnagle, G. Wallraff, D. Medeiros, G. Gallatin, J. Cobb, "Extendibility of Chemically Amplified Resists: Another Brick Wall?," *Proc. SPIE* **5039**, 1 (2003).
21. G. Schmid, M. Stewart, C. Wang, B. Vogt, V. Prabhu, E. Lin, C. Willson, "Resolution limitations in chemically amplified photoresist systems," *Proc. SPIE* **5376**, 333 (2004).
22. D. Fuard, M. Besacier, P. Schiavone, "Validity of the diffused aerial image model: an assessment based on multiple test cases," *Proc. SPIE* **5040**, 1536 (2003).
23. T. Brunner, C. Fonseca, N. Seong, M. Burkhardt, "Impact of resist blur on MEF, OPC, and CD control," *Proc. SPIE* **5377**, 141 (2004).
24. Y. Granik, D. Medvedev, N. Cobb, "Toward standard process models for OPC," *Proc. SPIE* **6520**, 652043 (2007).
25. *Fundamental Principles of Optical Lithography*, Chris Mack, John Wiley & Sons Ltd., West Sussex, England (2007).
26. Uzodinma Okoroanyanwu and J. H. Lammers, "Resist Road to the 22nm Technology Node", *Future Fab. Intl.* 17, Chapter 5, Section 5 (2004).

27. Hiroshi Fukuda, K. Hattori, and T. Hagiwara, “Impact of acid/quencher behavior on lithography performance”, Proceed. SPIE, 4346, 319-330, (2001).
28. R. Brainard, P. Trefonas, J. Lammers, C. Cutler, J. Mackevich, A. Trefonas, S. Robertson, “Shot noise, LER, and quantum efficiency of EUV photoresists”, Proceed. SPIE, 5374, 74-85, (2004)
29. C. Szamanda, et. al., “Measuring acid generation efficiency in chemically amplified resists with all three beams”, JVST B 17, 3356-3361, (1999);
30. Adam R. Pawlowksi, A. Acheta, H. Levinson, T. Michaelson, A. Jamieson, Y. Nishimura, C. Willson, “Line edge roughness and intrinsic bias for two methacrylate polymer resist systems”, J. Microlith. Microfab. Microsys. 5, 023001, (2006).

### List of Figures

**Fig. 1.** Three-dimensional representation of an example mask including the two roughness components of concern. Both the absorber LER and multilayer surface roughness are greatly exaggerated for illustrative purposes.

**Fig. 2.** Image of computed aerial image intensity given a mask matching the absorber and surface statistics of a typical EUV mask. The illumination condition is annular for an inner  $\sigma$  of 0.35 and an outer  $\sigma$  of 0.55 and the image is computed at best focus.

**Fig. 3.** LER power spectral density (PSD) and height-height correlation function computed from the aerial image after convolution with the resist PSF from Eq. [1]. No resist stochastic effects are included. Various  $R$  values are considered,  $k$  is assumed to be  $4 \text{ nm}^3/\text{s}$ , and  $t$  is 90 s. For comparison, the plots also show the PSD of typical resist roughness which is self-affine in nature.

**Fig. 4.** LER power spectral density (PSD) and height-height correlation function computed from the aerial image after convolution with the resist PSF from Eq. [1]. No resist stochastic effects

are included. Various  $k$  values are considered,  $R$  is assumed to be 15 nm, and  $t$  is 90 s. For comparison, the plots also show the PSD of typical resist roughness which is self-affine in nature.

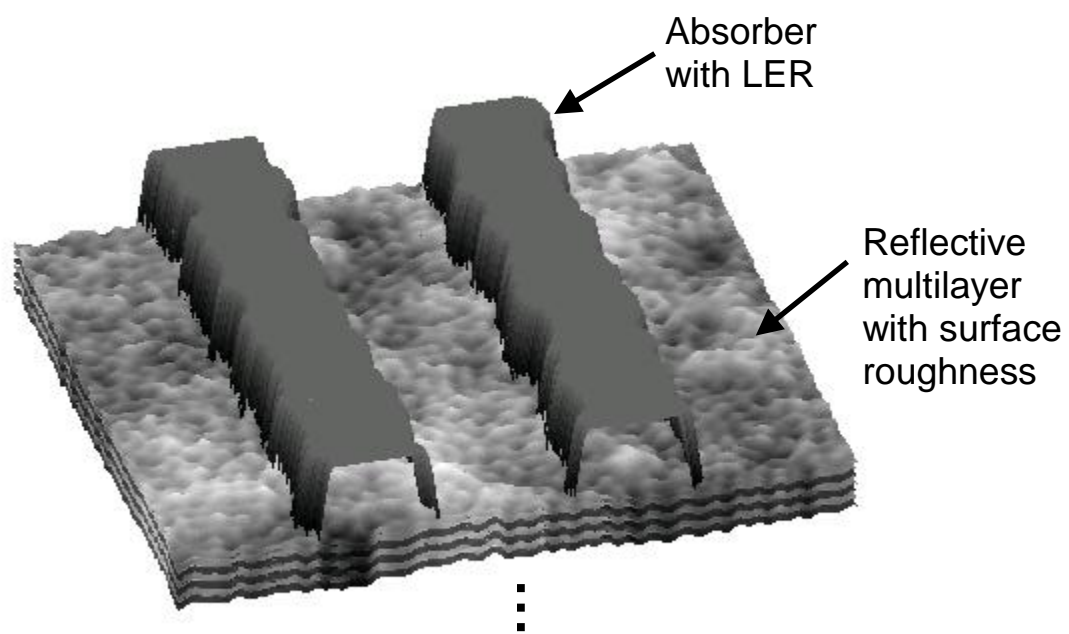
**Fig. 5.** LER power spectral density (PSD) and height-height correlation function after inclusion of resist stochastic effects assuming dose to size values of 2 mJ/cm<sup>2</sup>, 4 mJ/cm<sup>2</sup>, 8 mJ/cm<sup>2</sup>, 16 mJ/cm<sup>2</sup>, 32 mJ/cm<sup>2</sup>, 64 mJ/cm<sup>2</sup> and 128 mJ/cm<sup>2</sup>. The resist blur is set to 10 nm and deprotection rate is 4 nm<sup>3</sup>/s.

**Fig. 6.** Plots from Fig. 5 replotted on a normalized y axis to better visualize the change in the morphology or shape of the PSD and HHCF.

## List of Tables

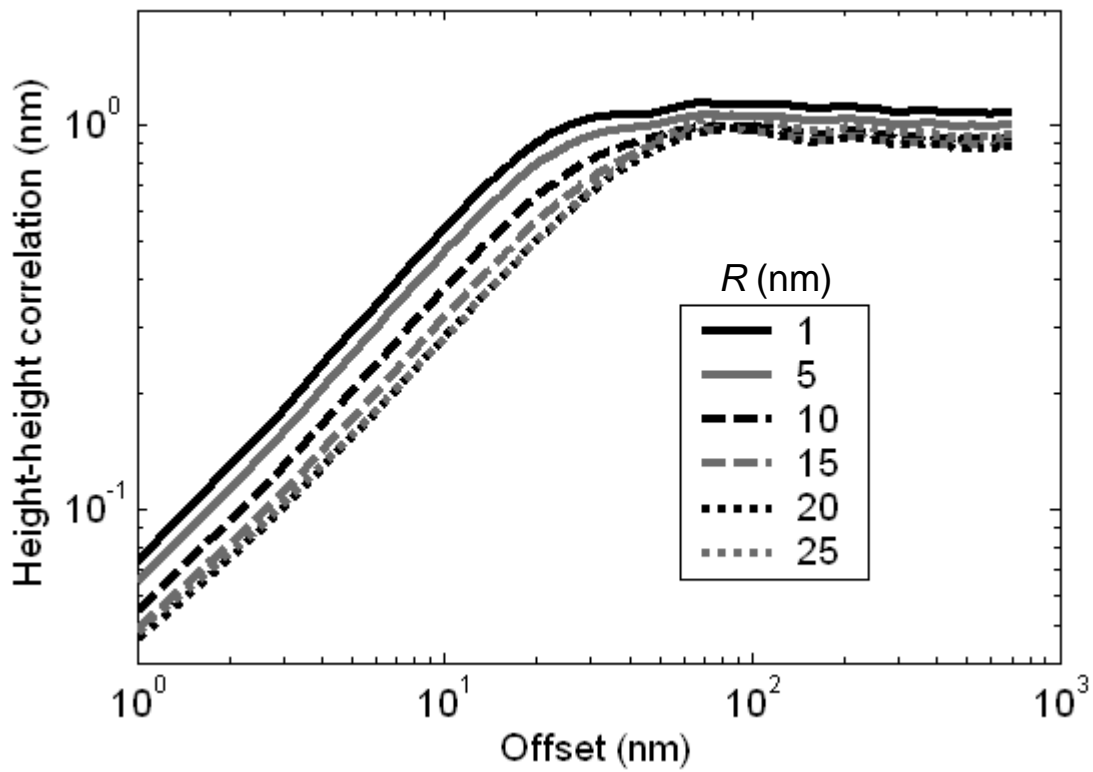
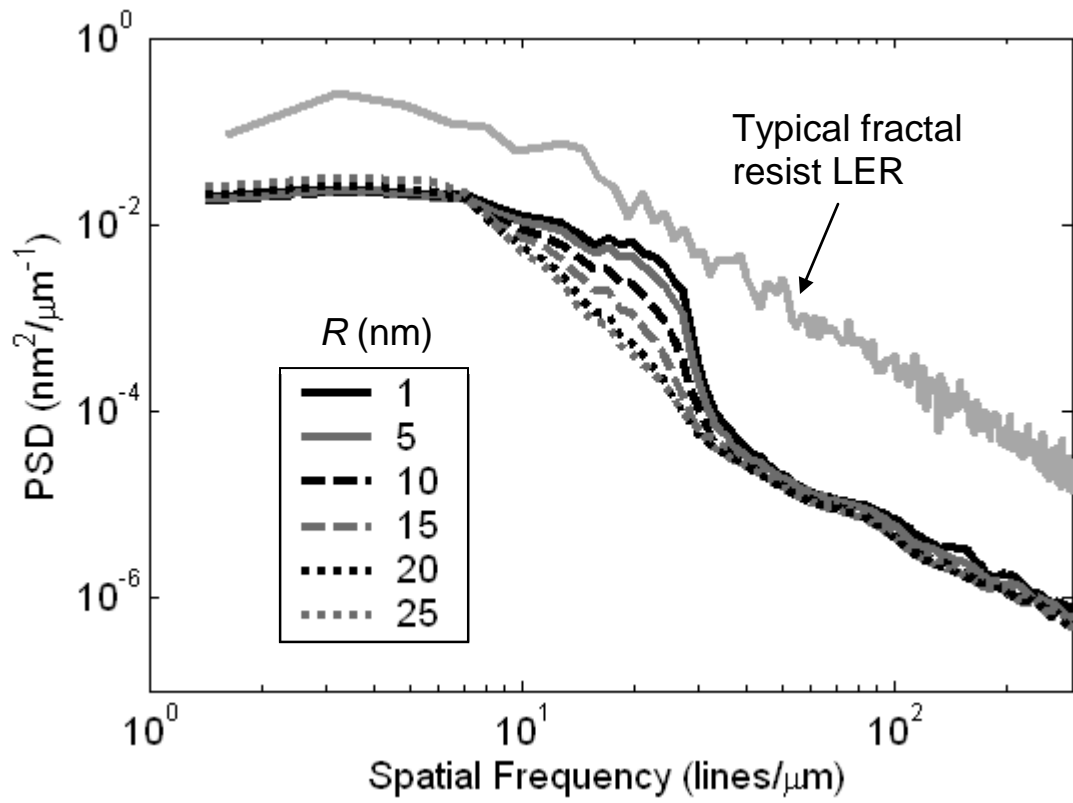
**Table 1.** Comparison of the roughness exponent measured from the PSD and HHCF for the various resist blur parameters used in Figs. 3 and 4. Also shown are the corresponding LER values. Although some effect on LER magnitude is observed due to the resist blur, it is negligible compared to the measurement uncertainty. The uncertainty values are three times the root-mean-square (rms) variation in the average LER for each blur parameter.

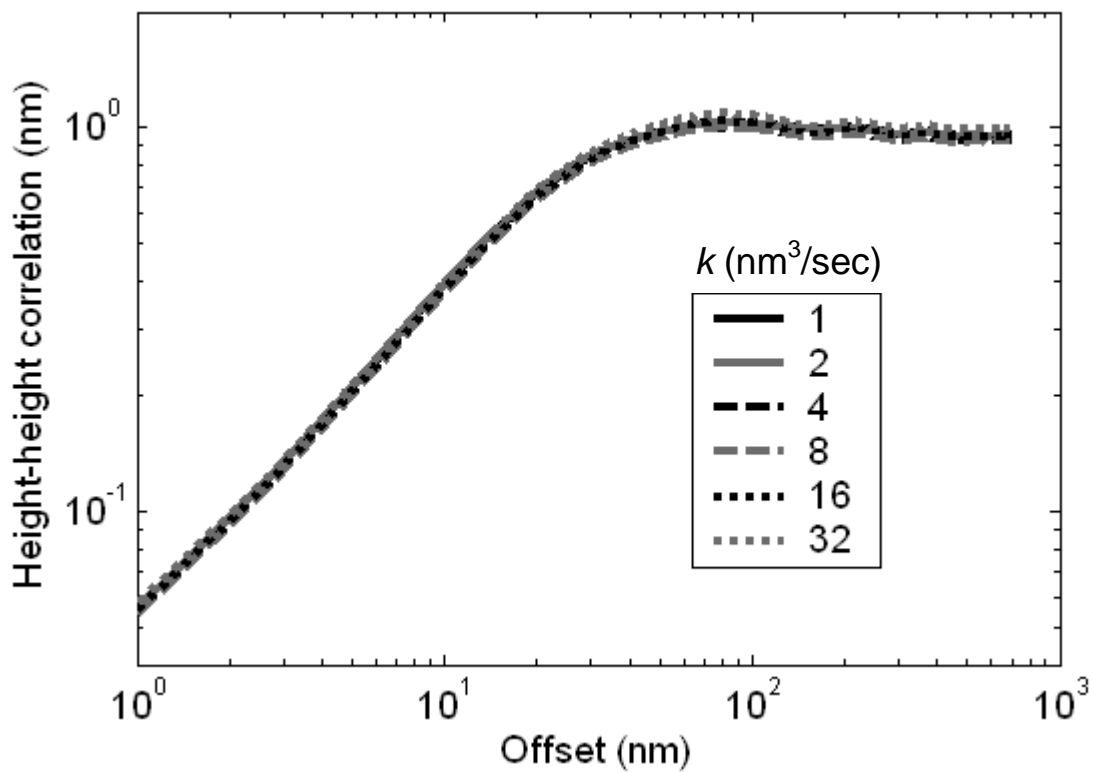
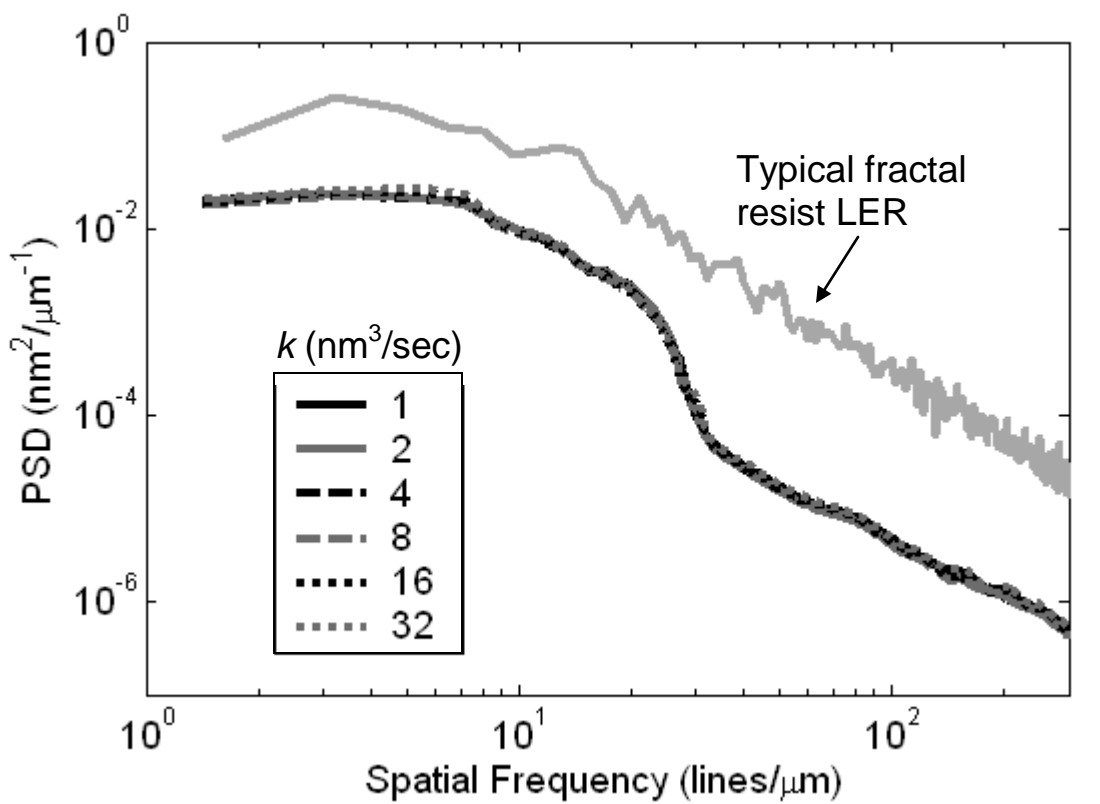
**Table 2.** Roughness exponent and LER as a function of sensitivity for model including both mask and resist effects. For dose to sizes below 16 mJ/cm<sup>2</sup>, we can no longer see evidence of the mask-induced LER in the roughness exponent. The mask effects only become evident when the mask-induced LER is so dominant that it accounts for nearly 100% of the total LER. The uncertainty values are three times the root-mean-square (rms) variation in the average LER for each sensitivity value.

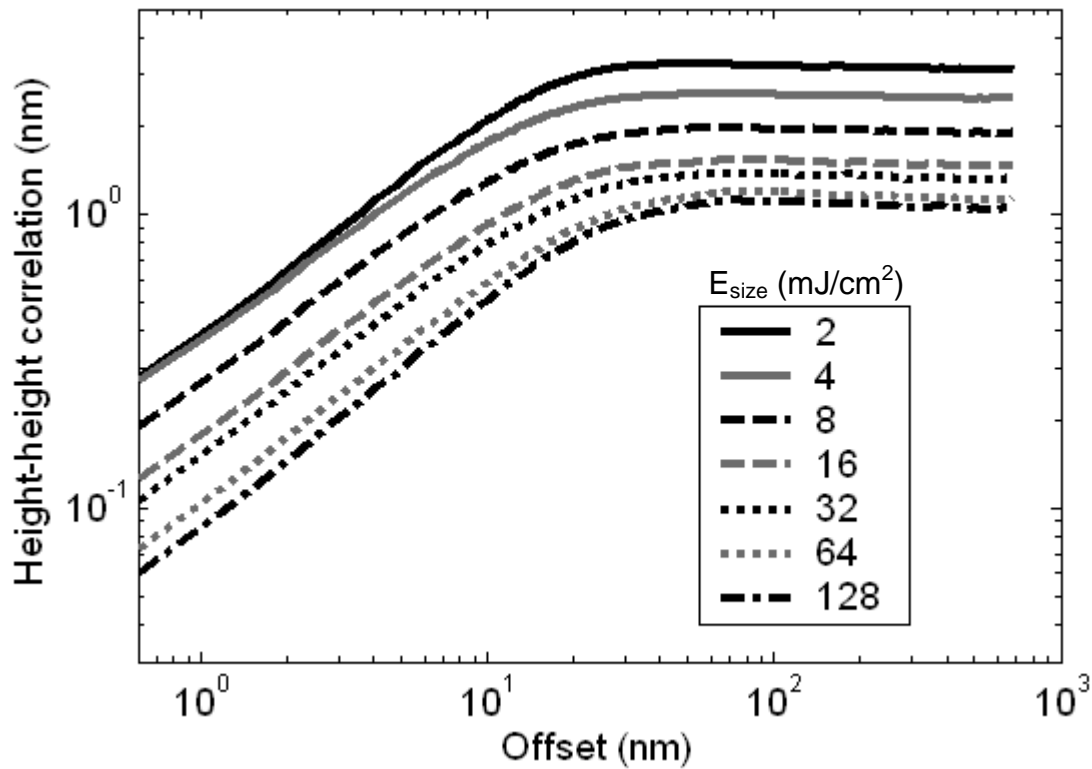
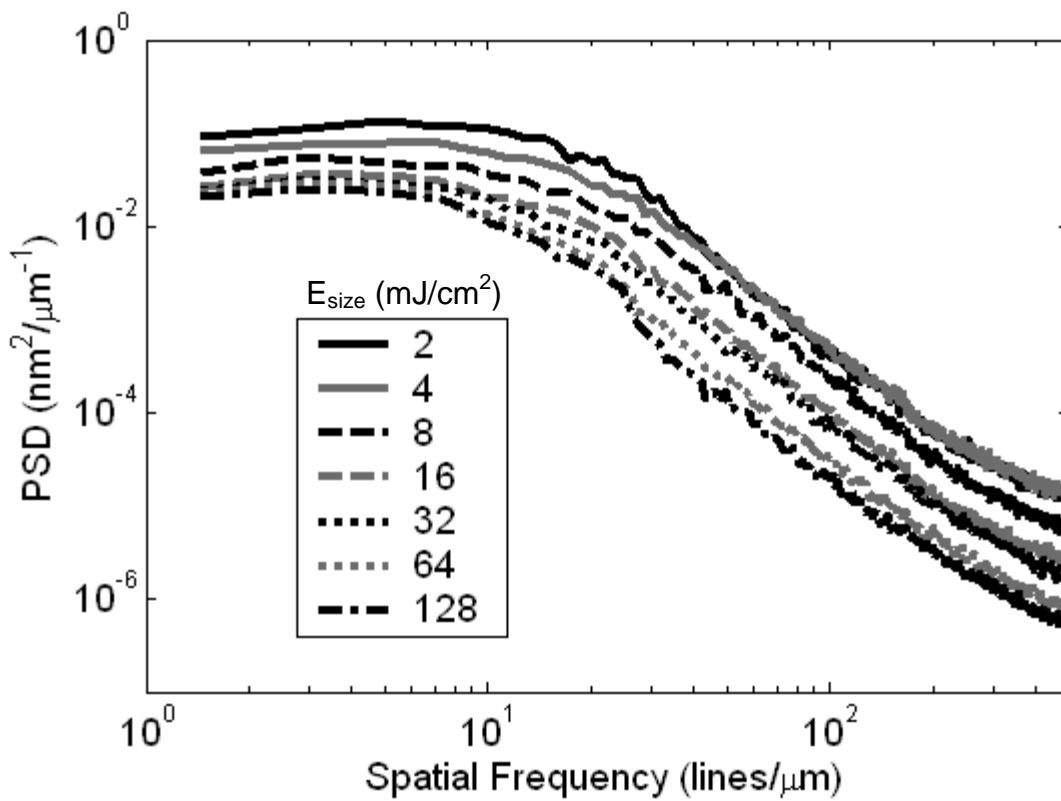


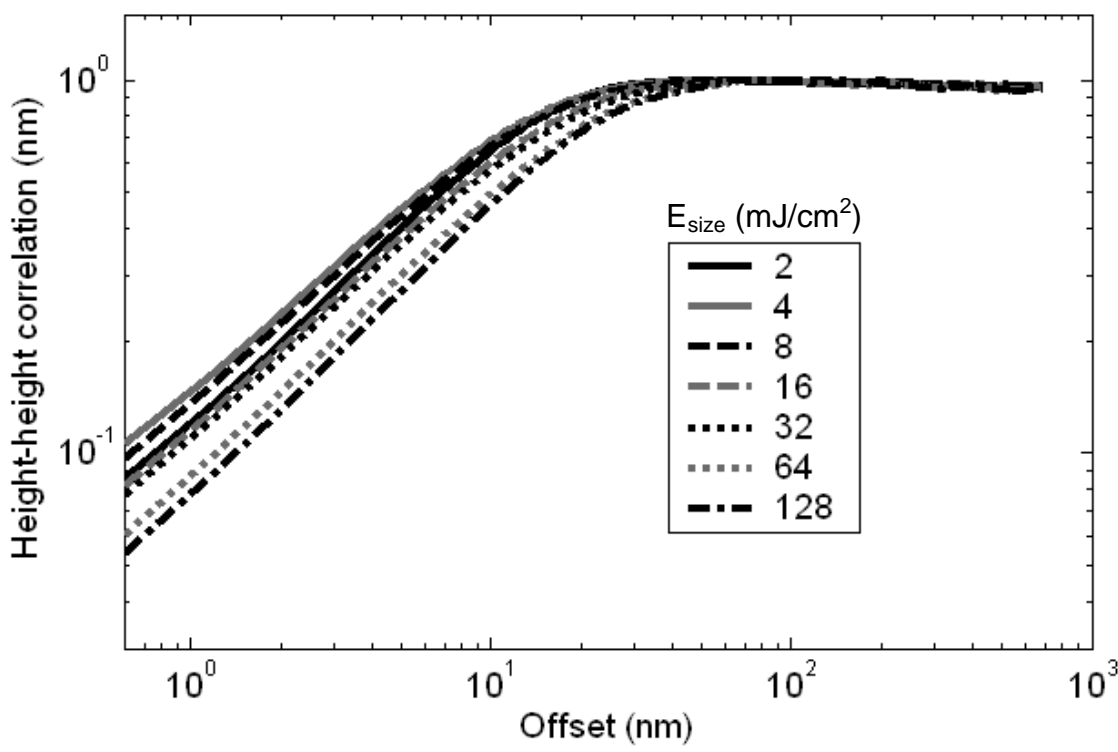
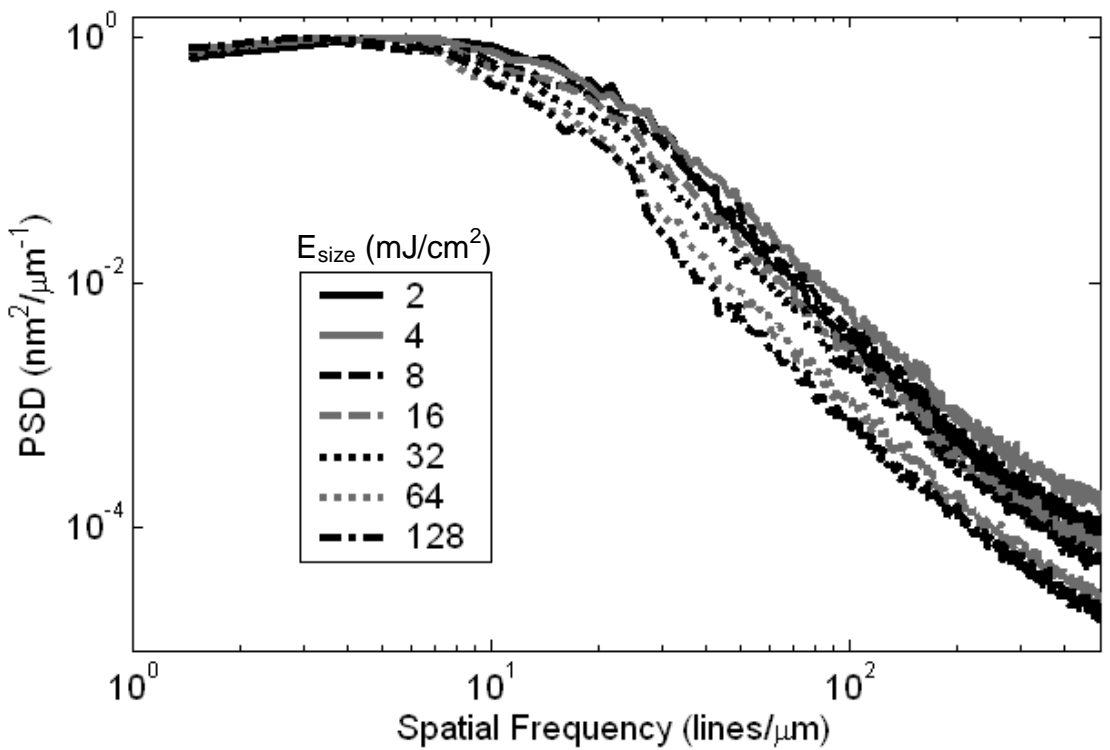
Naulleau and Gallatin, Fig. 2











Naulleau and Gallatin, Table 1

$k$ (nm <sup>2</sup> /s)	$R$ (nm)	$\alpha$ PSD	$\alpha$ HHCF	LER (nm)	LWR (nm)
NA	NA	0.12	0.88	2.2 ± 0.1	3.0 ± 0.1
4	1	0.50	0.88	2.3 ± 0.1	3.1 ± 0.1
4	5	0.42	0.87	2.2 ± 0.1	2.8 ± 0.1
4	10	0.55	0.85	2.0 ± 0.1	2.6 ± 0.1
4	15	0.48	0.84	1.9 ± 0.1	2.5 ± 0.1
4	20	0.51	0.83	1.9 ± 0.1	2.5 ± 0.1
4	25	0.51	0.82	2.1 ± 0.1	2.7 ± 0.1
1	10	0.46	0.86	2.1 ± 0.1	2.7 ± 0.1
2	10	0.60	0.86	2.1 ± 0.1	2.7 ± 0.1
4	10	0.55	0.85	2.0 ± 0.1	2.6 ± 0.1
8	10	0.50	0.85	2.0 ± 0.1	2.6 ± 0.1
16	10	0.50	0.85	2.1 ± 0.1	2.7 ± 0.1
32	10	0.57	0.85	2.2 ± 0.1	2.9 ± 0.1

Naulleau and Gallatin, Table 2

$E_{\text{size}}$ (mJ/cm <sup>2</sup> )	$\alpha$ PSD	$\alpha$ HHCF	LWR (nm)	LER (nm)
2	0.94	0.75	9.8 ± 0.1	6.7 ± 0.1
4	0.91	0.7	7.6 ± 0.1	5.3 ± 0.1
8	0.94	0.71	5.7 ± 0.1	4.1 ± 0.1
16	0.93	0.74	4.4 ± 0.1	3.2 ± 0.1
32	0.94	0.74	3.9 ± 0.1	2.8 ± 0.1
64	0.92	0.76	3.3 ± 0.1	2.4 ± 0.1
128	0.8	0.78	3.0 ± 0.1	2.3 ± 0.1